



Article

Nickel Ions Activated PbO–GeO₂ Glasses for the Application of Electrolytes and Photonic Devices

L. Vijayalakshmi ^{1,*}, Shaik Meera Saheb ², R. Vijay ³, Kishor Palle ⁴ , P. Ramesh Babu ⁵, Seong-Jin Kwon ^{1,*} 
and G. Naga Raju ⁶

¹ Department of Automotive Engineering, Yeungnam University, Gyeongsan-si 38541, Republic of Korea

² Department of Physics, Sai Spurthi Institute of Technology, B. Gangaram, Sathupally Mandal 507303, India

³ Department of Physics, Usha Rama College of Engineering & Technology, Telaprolu 521109, India

⁴ Department of H&S (Chemistry), CVR College of Engineering, Hyderabad 501510, India

⁵ Department of Physics, Gokaraju Rangaraju Institute of Engineering & Technology, Hyderabad 500090, India

⁶ Department of Physics, Acharya Nagarjuna University, Nagarjuna Nagar, Guntur 522510, India

* Correspondence: lvl.phy@gmail.com or drlvlphy@ynu.ac.kr (L.V.); sjkwon@yu.ac.kr (S.-J.K.)

Abstract: In this study, PbO–GeO₂ glasses were melt-quenched at different nickel oxide concentrations. XRD and DSC techniques were characterized whether the samples are glass or crystalline materials. IR, Raman, and optical absorption techniques are used to obtain structural details. The IR spectra have revealed that the glass network contained conventional structural units GeO₄ and GeO₆. The Ni²⁺ ion octahedral transition exhibited luminescence spectra in the region of 1200–1500 nm; it is due to ³T₂ (3F) → ³A₂ (3F) transition. The glasses containing the highest concentration of NiO have been found to have high values of luminescence efficiency and the cross-section. The dielectric characteristics, such as the dielectric constant, loss, and a.c. conductivity (σ_{ac}), were analyzed across extensive frequency and temperature ranges, with a specific emphasis on the nickel oxide concentration. Analyzing optical absorption and dielectric properties of the samples, it has been found that nickel ions' majority occur in tetrahedral sites. It is proved that the dielectric constant and loss values are highest for the sample N₁₀ and ac conductivity due to dipoles being lowest for the sample N₁₀. It is revealed that the glasses are highly conducting due to the modifying action of Ni²⁺ ions so these glasses are suitable for solid electrolyte uses besides their optical applications in NLO devices.

Keywords: lead germanium nickel oxide glasses; spectroscopic properties; dielectric properties



Citation: Vijayalakshmi, L.; Meera Saheb, S.; Vijay, R.; Palle, K.; Ramesh Babu, P.; Kwon, S.-J.; Raju, G.N. Nickel Ions Activated PbO–GeO₂ Glasses for the Application of Electrolytes and Photonic Devices. *Inorganics* **2024**, *12*, 215. <https://doi.org/10.3390/inorganics12080215>

Academic Editors: Pengwei Li and Yanfei Zhang

Received: 27 June 2024

Revised: 29 July 2024

Accepted: 7 August 2024

Published: 8 August 2024



Copyright: © 2024 by the authors. Licensee MDPI, Basel, Switzerland. This article is an open access article distributed under the terms and conditions of the Creative Commons Attribution (CC BY) license (<https://creativecommons.org/licenses/by/4.0/>).

1. Introduction

Glass plays a crucial role in various applications and technologies, making it an essential material in our daily lives. So, the glass industry was founded with the aim of creating a wide range of compounds for everyday use. In all these materials, the most important heavy metal oxide PbO in general behaves as a glass modifier. Upon entering into a glass network, the structure of the material changes. The low crystallization value and high moisture resistance are exposed by this information [1]. It has both a covalent and an ionic nature, which allows it to function as both a glass maker and a modifier [2]. The refractive index and melting point of materials are enhanced when lead oxide is introduced to the glass former. These types of glasses are utilized in situations where shielding, dispersion, and high refractive index are necessary [3]. The glassy nature is enhanced by [PbO₄] structural units whereas the network modifying action is due to [PbO₆] structural units of PbO. However, germanium oxide is commonly encountered in its vitreous state. It is considered a classic glass former and is known for its exceptional optical characteristics, including a refractive index (n~2.17). Moreover, it serves as an efficient transmitter in the near-infrared (NIR) region [4]. Germanium oxide glasses are used for making optical fibers and designing laser devices and in the field of nonlinear optics [5]. Since GeO₂ glasses have a high ionic conductivity, solid electrolytes are usually composed of them [6]. A structural

analysis of germanium oxide indicates that it is composed of structural units made up of GeO_4 and GeO_6 [7–9]. Depending on the type of bond between lead and oxygen atoms, the modifier PbO will act either as a network former or a modifier. Because of Pb ion high polarizability, a strong covalent Pb-O bond is formed between Pb^{2+} and O^{2-} ions [10]. Lead germanate glasses are promising candidates for optical amplifiers, and for numerous types of optical devices and high-speed optical switches containing nonlinearity [11].

The transition metal ions continue to be of interest for possible laser applications. Numerous transition metal activators have shown promise, particularly those that have led to successful lasers utilizing cation matrices. The existence and level of cations in glass have a notable influence on the key physical, structural, and chemical characteristics of these materials, encompassing electrical, magnetic, and optical properties [12,13].

Nickel containing glasses gained special attraction due to their interesting optical and dielectric properties; nickel exists in highly suitable Ni^{2+} ions, which mostly occupies octahedral sites in glasses with high crystal field energy [14]. There is no accurate evidence of change in its oxidation state during glass formation and annealing [15]. Visible and near-infrared region Ni^{2+} ions can show many absorption bands. The Ni^{2+} ions in octahedral configuration in a glass matrix can exhibit lasting action at about a 1.56 μm wavelength at room temperature. This wavelength is very important in telecommunications [16]. The zero-dispersion wavelength for GeO_2 is 1.7 μm (higher than that of borate, phosphate, or silicate glasses). The emission of laser beams in the near-infrared region is because of the existence of Ni^{2+} ions in the PbO-GeO_2 glass network [17]. In addition to being used in nonlinear optical devices, these glasses were also used in the preparation of broad band optical amplifiers, power limiters, optical amplifiers, ultrafast optical switches, and lasers [18,19]. The coordination of Ge would continuously change from GeO_4 to GeO_6 with the addition of alkali oxides. Recently, the structural properties of germanate-based glasses have been examined in $\text{Na}_2\text{O-GeO}_2\text{-TeO}_2$ [20], $\text{MnO-GeO}_2\text{-PbO}_2$ [21], $\text{TeO}_2\text{-GeO}_2\text{-PbO}$ [22], $\text{Na}_2\text{CO}_3\text{-CaO-GeO}_2$ [23], and $\text{Ga}_2\text{O}_3\text{-GeO}_2\text{-BaO}$ [24]. Among the reported germanate-based glasses, the lead germanate matrix has received the most attention due to its excellent properties, i.e., a relatively large glass-forming region, high transmittance in a wide wavelength region, superior chemical durability, and thermal stability [25,26].

Very little work was reported about nickel oxide-doped lead germanate glasses; moreover, work on the dielectric properties of dense glass systems like PbO-GeO_2 glasses is very strange. So, the present work is aimed to report spectral features and dielectric studies of a nickel oxide-doped PbO-GeO_2 glass system by means of spectroscopic techniques and electrical measurements, thereby comprehending the environment of nickel ions and explaining suitability of these glasses for specific uses as electrolytes.

2. Results

From the measured density values of PbO-GeO_2 glass samples, various other physical parameters such as polaron radius r_p and nickel ion concentration N_i are calculated and presented in Table 1. As the concentration of nickel oxide increases, the density of the samples is also increased. The structural variations in the glass network are investigated by physical properties of the samples.

Table 1. Summary of the data physical parameters of the PbO-GeO_2 : NiO glasses.

Glass Sample	Density d (g/cm^3)	Molar Volume V_m (cm^3)	Nickel Ion Conc. N_i ($\times 10^{21}/\text{cm}^3$)	Inter-Ionic Distance of Nickel Ions R_i (Å)	Polaron Radius R_p (Å)
N_0	5.56	0.520	--	--	--
N_2	6.035	0.886	4.78	5.93	2.39
N_4	6.054	0.586	9.60	4.70	1.89
N_6	6.072	0.953	14.44	4.10	1.654
N_8	6.08	1.008	19.29	3.72	1.50
N_{10}	6.15	0.908	24.41	3.44	1.38

Figure 1 illustrates the amorphous structure of the samples, as demonstrated by the absence of Bragg peaks in X-ray diffraction patterns.

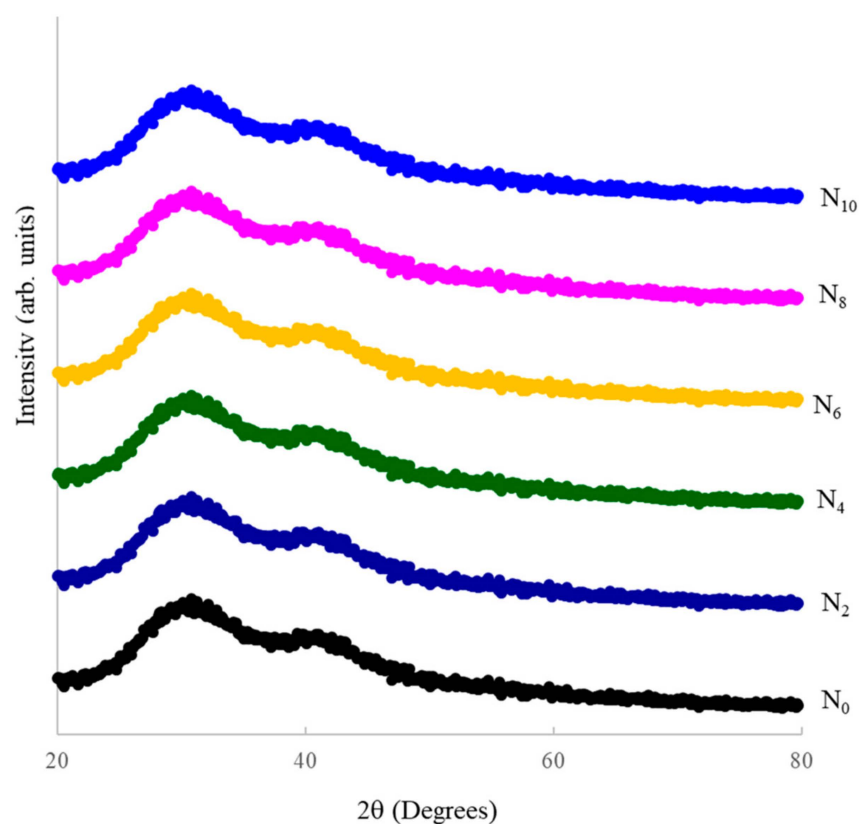


Figure 1. XRD patterns of PbO–GeO₂: NiO glasses.

Figure 2 displays the differential scanning calorimetric traces of the PbO–GeO₂ glass system doped with nickel oxide, along with the glass-forming ability parameter (K_{gl}) and the variation of glass transition temperature (T_g) as indicated in the inset. The pattern demonstrates fluctuations in T_g in the temperature range of 490 to 510 °C with an endothermic effect. Additionally, an exothermic effect is observed due to the crystallization temperature T_c , which falls in the range of 615 to 630 °C. The DSC data in Table 2 illustrate the changes in (T_g), ($T_c - T_g$), ($T_m - T_c$), and (K_{gl}) [27] of PbO–GeO₂ glasses as they are doped with varying nickel oxide concentrations. It has been observed that the glass-forming ability parameter K_{gl} decreases as the concentration of nickel oxide increases. This trend may be attributed to the alterations in the glass composition and structural properties resulting from the addition of nickel oxide.

Table 2. DSC data of PbO–GeO₂ glasses doped with different concentrations of NiO.

Glass	T_g (°C)	T_c (°C)	T_m (°C)	$T_c - T_g$ (°C)	$K_{gl} =$ $(T_c - T_g)/(T_m - T_c)$
N ₀	497	627	762	130	0.963
N ₂	499	625	763	126	0.913
N ₄	503	623	766	120	0.834
N ₆	505	622	769	117	0.796
N ₈	506	619	771	113	0.743
N ₁₀	504	615	772	111	0.707

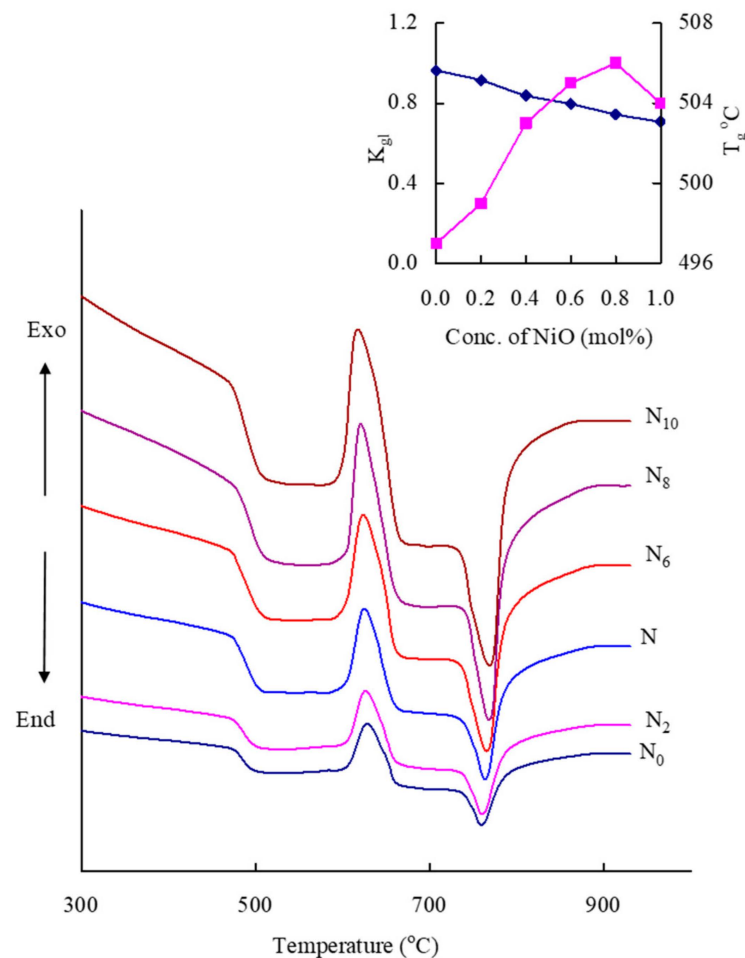


Figure 2. DSC patterns of PbO–GeO₂: NiO glasses. The inset shows the variation of T_g and K_{gl} with the concentration of NiO.

As shown in Figure 3, titled glass samples were investigated in the 350–1550 nm wavelength range at room temperature. Between 700 nm and 820 nm, a prominent band was observed in these spectra. The width and height are increased with increasing the content of NiO in these spectra. Regarding influences of Ni²⁺ ions, a number of absorption bands are observed. In the visible and NIR regions, 1.0 mol% glass (N₁₀) shows six evidently resolved absorption bands at 1265 nm (O_{h1}), 1029 nm (T_{d1}), 781 nm (O_{h2}), 623 nm (T_{d2}), 495 nm (O_{h3}), and 421 nm (O_{h4}) [28,29]. When the concentration of nickel increases, the intensity of octahedral bands is increased while tetrahedral bands are observed to decrease.

We calculated optical band gaps (E_o) of samples from cutoff wavelengths by using the relation

$$(\alpha\hbar\omega)^2 = C(\hbar\omega - E_o) \quad (1)$$

where α is the absorption coefficient (cm⁻¹), $\hbar\omega$ is photon energy of incident radiation (eV), E_o is the optical band gap energy (eV), and C is the band tailing parameter.

Figure 4 indicates that the Tauc plots and inset give optical band gap variation with concentration. Using the linear portion as a reference, E_o values are determined as shown in Table 3; the maximum E_o value is observed for the N₂ glass sample.

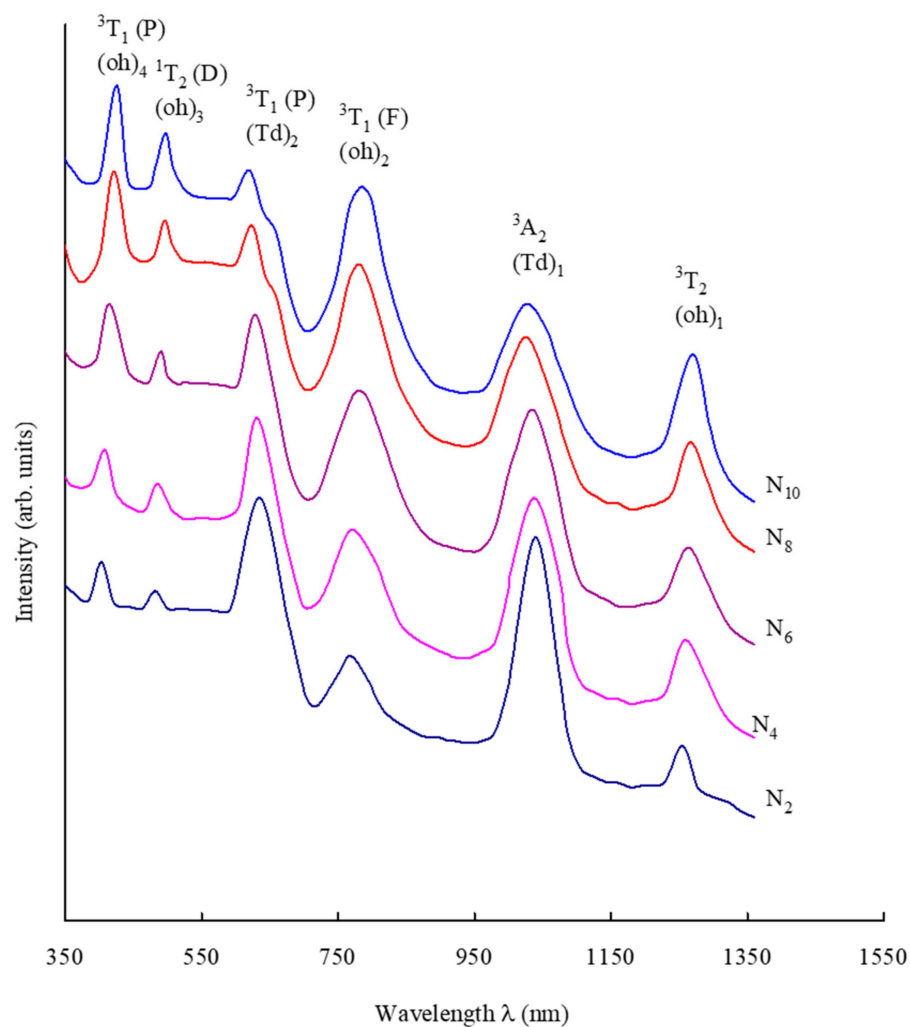


Figure 3. Optical absorption spectra of PbO-GeO₂ glasses doped with nickel oxide.

Table 3. Summary of the data related to optical absorption spectra of the PbO-GeO₂: NiO glasses.

Band Position (nm)	N ₂	N ₄	N ₆	N ₈	N ₁₀
Ni ²⁺ band positions, octahedral transitions (nm)					
${}^3A_2(F) \rightarrow {}^3T_2(F)$	1254	1258	1262	1265	1269
${}^3A_2(F) \rightarrow {}^3T_1(F)$	769	771	774	781	784
${}^3T_2(F) \rightarrow {}^1T_2(D)$	482	484	490	495	497
${}^3A_2(F) \rightarrow {}^3T_1(P)$	403	408	415	421	425
Ni ²⁺ band positions, tetrahedral transitions (nm)					
${}^3A_2(F) \rightarrow {}^3A_2(F)$	1040	1038	1034	1029	1024
${}^3A_2(F) \rightarrow {}^3T_1(F)$	635	631	628	623	620
Optical band gap E _o (eV)	2.58	2.51	2.36	2.32	2.27

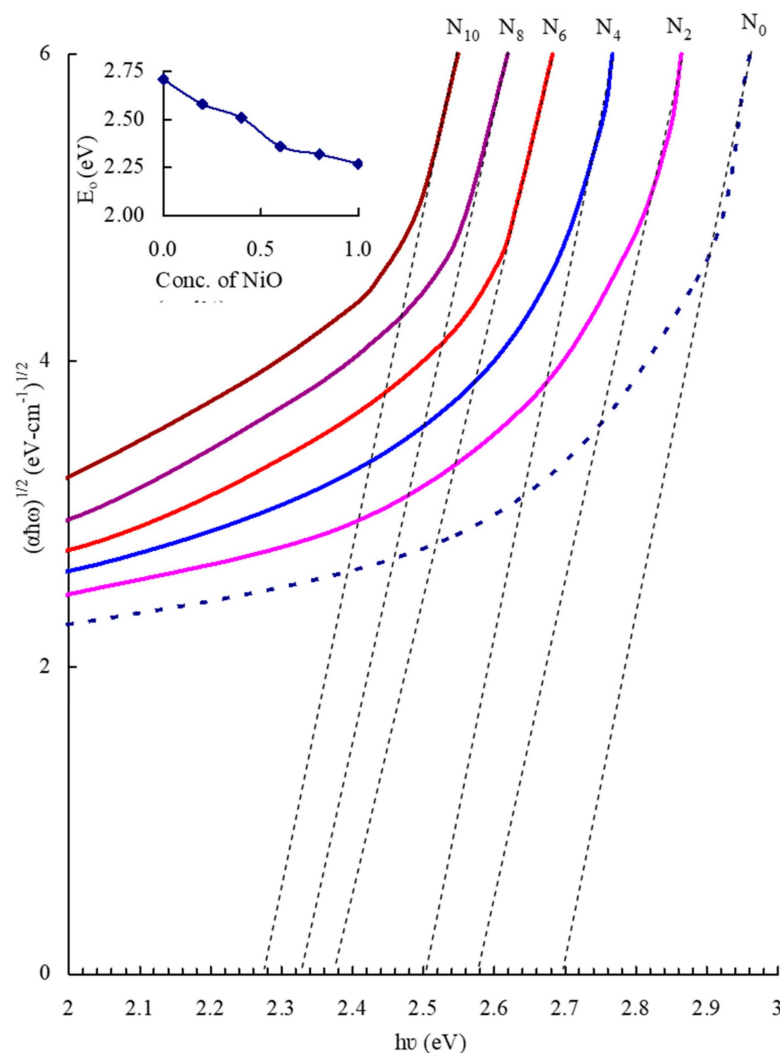


Figure 4. Tauc plots of PbO–GeO₂: NiO glasses. The inset represents the variation of the optical band gap with the concentration of NiO.

The FTIR spectra have been depicted in Figure 5. These spectra exhibit two crucial bands that correspond to the tetrahedral and octahedral vibrations of GeO₂ at 1075 and 780 cm⁻¹, respectively. Because of GeO₆ and GeO₄ units, asymmetrical stretching vibrations regarding these bands are located [18]. One more band is observed due to bonding between two tetrahedral groups at 642 cm⁻¹ [19,30]. The PbO₄ tetrahedral units are located at about 448 cm⁻¹ [18]. Intensity of GeO₆ and Ge–O–Ge of GeO₂ bands decreased and shifted gradually towards higher frequencies; similarly, GeO₄ and PbO₄ bands shifted towards lower frequencies with increased intensity with the introduction of nickel oxide into the glass network. The FTIR bands are shown in Table 4.

The Raman spectra of PbO–GeO₂: NiO are shown in Figure 6. These spectra contained symmetric Ge–O–Ge bands due to Q⁴ units of GeO₄ in between the 420 and 450 cm⁻¹ region [31], a vibrational band of Q³ units of GeO₄ in the region 520–540 cm⁻¹, a vibrational band of GeO₆ blocks at 620 cm⁻¹ [32], and two weak bands due to Q² and Q¹ blocks of GeO₄ at 900 and 960 cm⁻¹, respectively. PbO₄ exhibited blocks at 280 cm⁻¹. A high intense vibrational band of localized Ge–O⁻ stretching of the meta-germanate blocks at around 750 cm⁻¹ and no bands are exhibited by NiO units. The information regarding the band positions of Raman spectra can be found in Table 5.

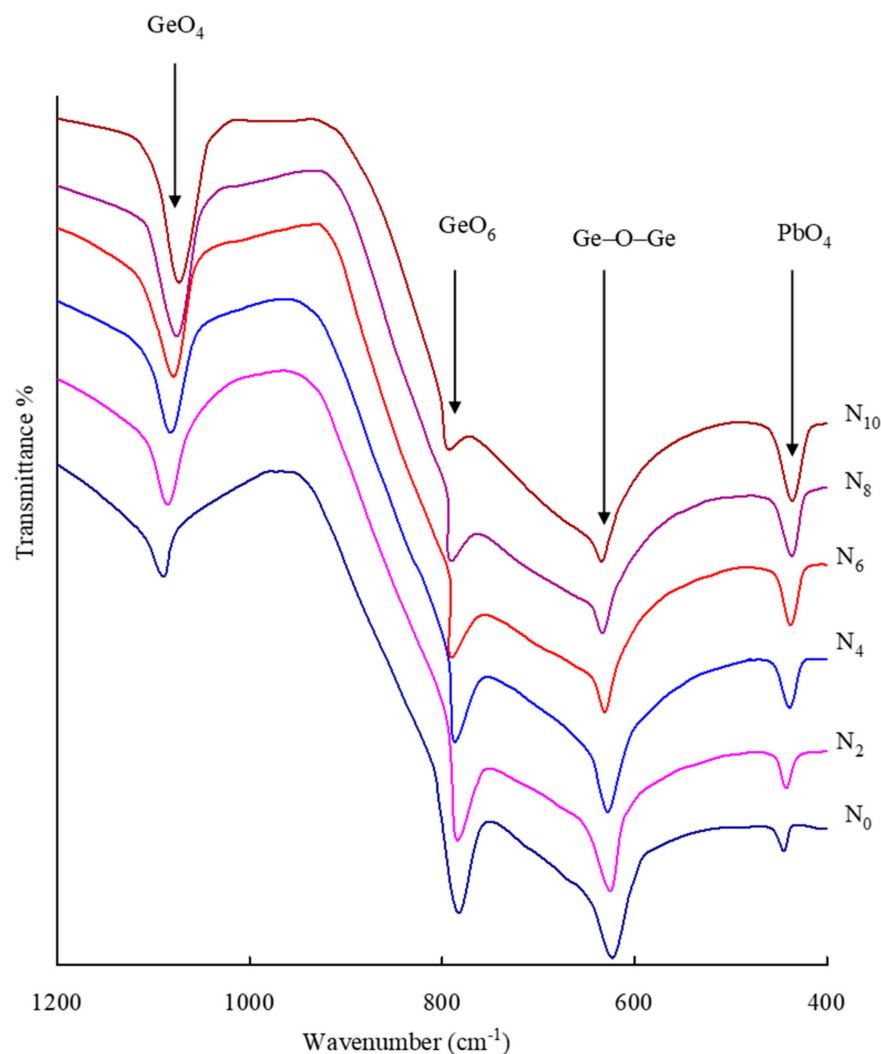


Figure 5. FTIR spectra of PbO–GeO₂ glasses doped with nickel oxide.

Table 4. Summary of the band positions (cm^{−1}) of various structural units in FT-IR spectra of PbO–GeO₂: NiO glasses.

Glass	GeO ₄ Units	GeO ₆ Units	Ge–O–Ge Bending Vibrations	PbO ₄ Units
N ₀	1088	783	622	445
N ₂	1085	785	625	442
N ₄	1080	787	627	439
N ₆	1077	791	631	437
N ₈	1075	792	633	436
N ₁₀	1072	794	634	435

Photoluminescence spectra of PbO–GeO₂: NiO glasses are shown in Figure 7. Photoluminescence spectra of nickel oxide were recorded at 300 K with $\lambda_{\text{exc}} = 800$ nm. In the wavelength region 1200–1500 nm, the spectra exhibited a wider emission for all the samples due to the ${}^3T_2(3F) \rightarrow {}^3A_2(3F)$ transition of Ni²⁺ ions. The intensities and line widths of the band increase with nickel oxide concentration as shown in Table 6, while the peaks shift toward higher wavelengths.

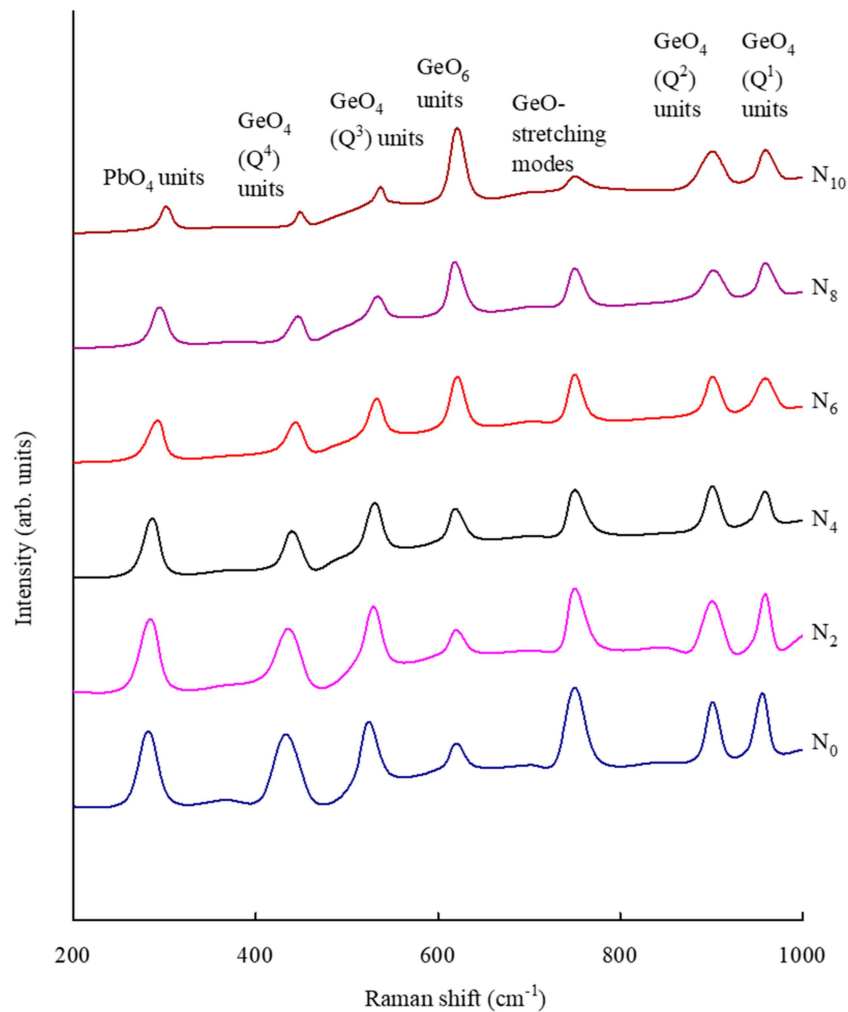


Figure 6. Raman spectra of PbO–GeO₂ glasses doped with nickel oxide.

Table 5. Summary of the data on band positions (cm⁻¹) of Raman Spectra of PbO–GeO₂: NiO glasses.

Glass	PbO ₄	GeO ₄ (Q ⁴) Units	GeO ₄ (Q ³) Units	GeO ₆ Units	GeO ⁻ Units	GeO ₄ (Q ²) Units	GeO ₄ (Q ¹) Units
N ₀	282	433	524	621	750	901	959
N ₂	284	436	529	620	750	901	959
N ₄	286	440	530	619	750	901	959
N ₆	292	443	532	618	750	901	959
N ₈	294	446	534	618	750	901	959
N ₁₀	301	448	537	618	750	901	959

Table 6. Summary of data on photoluminescence of PbO–GeO₂: NiO glasses.

Sample	Emission Peak Position (nm)	Refractive Index	σ_p^E (10 ³³ , cm ²)
N ₂	1303	1.542	0.932
N ₄	1306	1.545	0.934
N ₆	1309	1.549	0.939
N ₈	1313	1.552	0.943
N ₁₀	1316	1.556	0.945

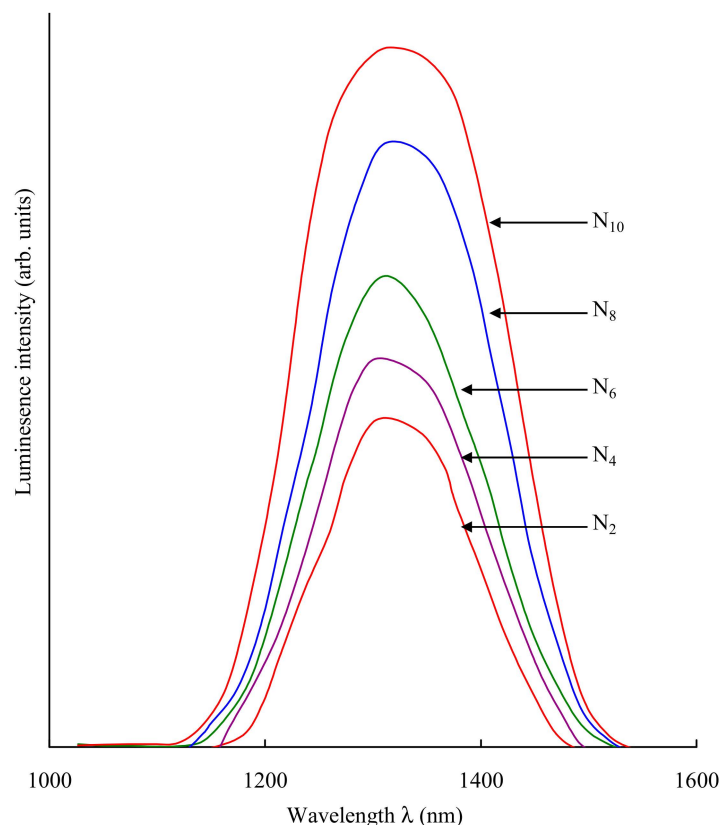


Figure 7. Photoluminescence of PbO–GeO₂ glasses doped with nickel oxide recorded at room temperature ($\lambda_{\text{exc}} = 800$ nm).

The variation of ϵ' versus temperature graphs of the glasses is shown in Figure 8. At higher temperature and lower frequencies, slight increases in the dielectric constant were observed and it increases abruptly with temperature. It should be high for glass N₁₀. Figure 9 shows the temperature versus $\tan \delta$ graphs of glass samples at different frequencies. The curves have shown a maximum value of $\tan \delta$ for the glass N₁₀. The σ_{ac} values are obtained by changing temperature using the following equation:

$$\sigma_{ac} = \omega \epsilon^1 \epsilon_0 \tan \delta \quad (2)$$

where σ_{ac} is ac electrical conductivity (S/m), ω is angular frequency (s^{-1}), and ϵ^1 is the dielectric constant.

Figure 10 represents the plots of ac conductivity, σ_{ac} , with $1/T$ and is drawn at 100 kHz for all the glasses. The inset of Figure 10 explains the variation of activation energy with changes in electrical conductivity σ_{ac} . N₁₀ has shown the lowest value of activation energy as presented in Table 7.

Table 7. Data on dielectric parameters of PbO–GeO₂: NiO glasses.

Glass	A.E for Conduction (eV)	σ_{ac} (10^{-7}) ($\Omega \text{ cm}$) ⁻¹
N ₀	0.43	0.56
N ₂	0.39	0.77
N ₄	0.36	1.08
N ₆	0.33	1.59
N ₈	0.29	2.54
N ₁₀	0.25	4.22

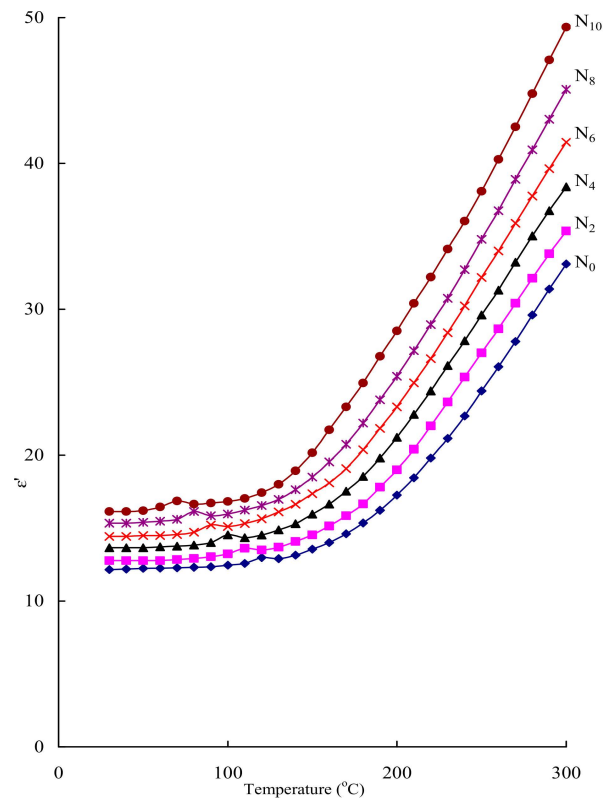


Figure 8. The dispersion of the dielectric constant, ϵ' , vs. temperature at 100 kHz for the glasses PbO-GeO₂ doped with different concentrations of nickel oxide.

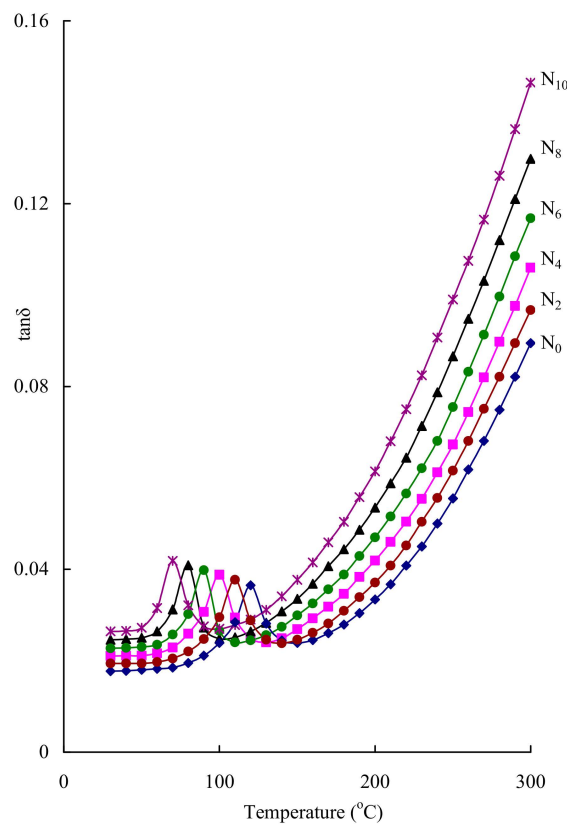


Figure 9. The variation of dielectric loss with temperature at 10 kHz frequency for the glasses PbO-GeO₂ doped with different concentrations of NiO.

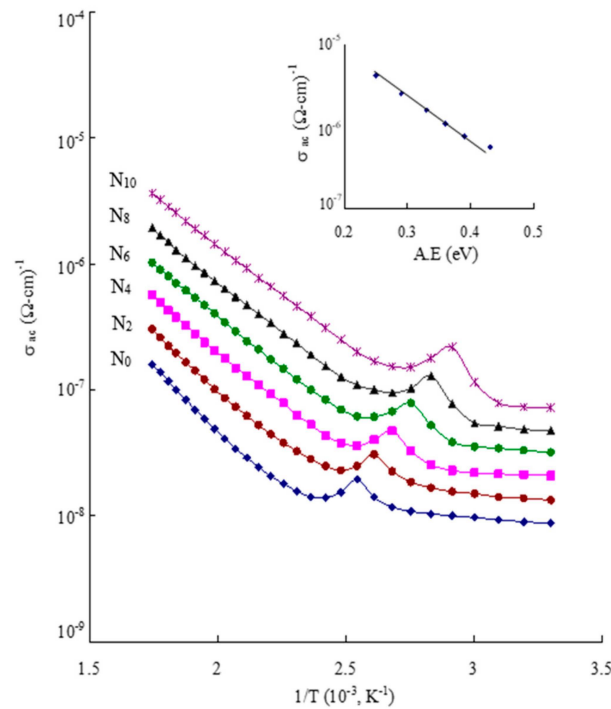


Figure 10. The variation of ac conductivity with $1/T$ at 100 kHz of PbO–GeO₂ glasses doped with nickel oxide. The inset represents the variation of ac conductivity regarding the activation energy.

It is verified that the σ_{ac} increased as activation energy (A.E) decreased, following the Arrhenius equation.

$$\sigma_{ac} = \sigma_0 e^{-E_a/KT} \tag{3}$$

where σ_{ac} is ac electrical conductivity (S/m) and σ_0 is conductivity at zero Kelvin.

E_a is activation energy (eV), T is temperature, and K is the Boltzmann constant.

The variation of the $4\pi N\mu^2/27 K$ value with nickel oxide concentration is shown in Figure 11.

$$\frac{\epsilon_s - \epsilon_\infty}{(\epsilon_s + 2)(\epsilon_\infty + 2)} T = \frac{4\pi N\mu^2}{27K} \tag{4}$$

where ϵ_s is the low-frequency dielectric constant, ϵ_∞ is the high-frequency dielectric constant, $N\mu^2$ is the strength of dipoles (C^2m^{-1}), and K is the Boltzmann constant.

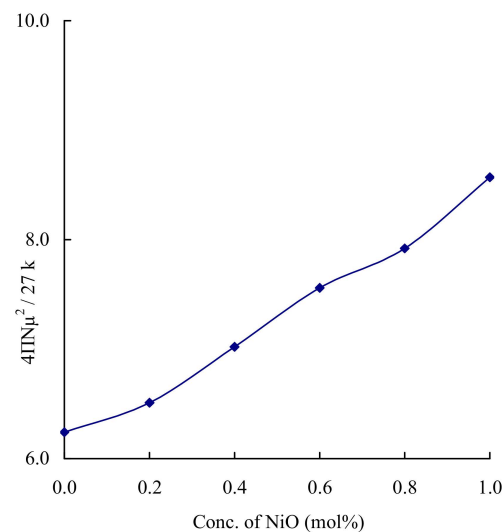


Figure 11. Dependence of $4\pi N\mu^2/27 K$ on concentration of nickel oxide.

$N\mu^2$ is the strength of dipoles. For various concentrations of nickel oxide, the values of ϵ_s and ϵ_∞ subsisting in the above equation and $4\pi N\mu^2/27 K$ are calculated at 393 K. The curve has shown a rising trend with nickel oxide concentration.

3. Discussion

In the PbO–GeO₂ glass system, the presence of GeO₂ in conjunction with GeO₄ tetrahedra within the network of the glass can lead to the conversion of a few tetrahedral units into GeO₆. There is typically one GeO₆ octahedron separated by one GeO₄ tetrahedron that shares one oxygen corner. Studies on GeO₂ glasses have revealed interactions between the GeO₅ structural units and germanium ions, where four bonds are of shorter length (ranging from 1.76 to 1.85 Å) and one bond has a longer interatomic distance of 1.92 Å.

The stretching of GeO₄ tetrahedra of a Ge–O bond is induced by the modifier PbO. As a result, the presence of Pb ions leads to the formation of three-membered rings in the vicinity of GeO₄ tetrahedra. The results revealed that Ge ions also participated in the glass structure with germanium dioxide network units. In addition, the infrared spectra have shown that there are bonds between GeO₄ and PbO₄, PbO₂, PbO₅, and PbO₆ structural units [33]. Lead oxide is a glass modifier; it forms Ge–O–Ge linkages by entering into the glass structure along with NBOs and dangling bonds. When lead ions form four covalent bonds with oxygen atoms, they can form structural units called [PbO₄] and [PbO₂]. [PbO₅] and [PbO₆] are produced by the lead ions and form Ge–O–Pb linkages whereas the Ni²⁺ acts as a network modifier. Transition metal ions, including Ni²⁺, are known to influence the structural, optical, and electrical properties of glasses significantly. Ni²⁺ can act as a network modifier by occupying interstitial sites and creating non-bridging oxygens (NBOs), thus altering the glass matrix's connectivity and properties. In our study, Ni²⁺ ions are introduced into the PbO–GeO₂ glass network, primarily occupying octahedral sites. The observed spectroscopic features and the dielectric properties of the glasses support this conclusion. Our findings are consistent with previous research that highlighted similar roles for transition metal ions in glass systems [34].

Usually, the density of glass samples depends on glass structure, size of grains, coordination number of glass-forming ions, size of interstitial spaces, etc. The density of samples is increased with the content of NiO, indicating its higher compactness for the N₁₀ sample.

The absence of sharp Bragg peaks indicates that the samples are in short-ranged structured materials (amorphous in nature). The glass-forming ability ($T_c - T_g$) decreased as the content of nickel oxide increased. So, it is proved that the lowest nickel oxide content is preferred for suitable glasses. It is inferred that glass samples with lower values will have less thermal stability. The decrease in interatomic distance, cross-linking, and closely packed structure are the reasons for such a behavior. Further, it is justified that the Ni²⁺ ions mostly acted as a modifier in (O_h) configuration as the NiO content is increased.

According to Tanabe–Sugano notation, the transitions of the d⁸ ion of nickel are mentioned below: ³A₂(F) → ³T₂(F) (O_{h1}), ³T₁(F) (O_{h2}), ¹T₂(D) (O_{h3}). The ³A₂(F) → ¹T₂(D) corresponds to a spin forbidden band at 570 nm while the band at 530 nm is due to ³A₂(F) → ³T₁(P) tetrahedral transition [35]. The increasing intensity in the octahedral bands with an increase in the mol% of NiO proved the presence of octahedrally bonded Ni²⁺ ions in a large number rather than the tetrahedrally bonded Ni²⁺ ions.

The optical band gap decreases as nickel oxide concentration increases. With an increase in doping levels, Ni²⁺ ion donor centers in a large number are produced. So, the excited states of local electrons superpose with the unfilled 3d states of nearby Ni²⁺ sites. This causes the nickel oxide band to extend into the main band gap to a greater extent. From N₂ to N₁₀, the band gap has fallen due to the shift of cutoff wavelengths to a higher wavelength side.

The GeO₆ band intensity is increased with an increasing concentration of nickel oxide. This indicates that nickel ions are located in the glass structure in an octahedral fashion. In addition to the wavelength shift of the octahedral bands, nickel oxide doping also increases

the wavelength shift. This shift in the band position indicated higher bond length of the Ni–O bond.

The IR spectra indicate the presence of symmetrical and anti-symmetrical bands corresponding to germanate structural units. The nickel oxide concentration is inversely proportional to the intensity of symmetric (GeO_6) units. Due to Ge–O–Ge symmetric vibrations, the intensity of bands decreases and anti-symmetrical bands due to (GeO_4) have increased as shown in Table 4. These results suggested decreasing entropy in the glass network with a hike in nickel oxide content.

It has been observed that Ge–O–Ge bonds of Q^2 and Q^1 units of GeO_4 show weak asymmetric stretching at about 900 and 960 cm^{-1} in Raman spectra. It was observed that the meta-germanate Ge-O^- unit stretching modes showed a strong vibrational band at around 750 cm^{-1} .

In the region 430 and 520 cm^{-1} , GeO_4 exhibits symmetric Ge–O–Ge bands due to the Q^4 unit and a vibrational band of the Q^3 unit. Additionally, a vibrational band of GeO_6 and PbO_4 blocks are observed at 620 and 280 cm^{-1} . No bands are exhibited by nickel oxide. The intensity of asymmetric stretching vibrations of GeO_6 units is increased at the expense of symmetric stretching vibrations regarding GeO_4 units in the Raman spectra. The concentration of nickel oxide increases and evidently suggested disorder in the glass network decreases.

In general, octahedral nickel ions produce photoluminescence, and tetrahedral nickel ions have no photoluminescence. In the green, red, and near-infrared (NIR) wavelength ranges, the octahedral Ni^{2+} ions produce luminescence bands [36]. For our samples, $\lambda_{\text{exc}} = 800\text{ nm}$ and the band ranges from 1200 to 1500 nm and the meta-center shifts towards a higher wavelength with an increase in nickel oxide content. The Stokes shift increases between higher and lower bands. The value of the emission cross-section σ_p^E has been computed and tabulated. Increasing the content of nickel oxide, the value of σ_p^E is found to increase gradually from N_2 to N_{10} , proving the increase in luminescence efficiency.

Electronic, ionic, dipolar, and interfacial polarizations are the different types of polarizations. These polarizations can influence the relative permittivity ϵ' and interfacial polarization is a response to the structure of glasses. The value of interfacial polarization depends on the dielectric parameters (ϵ' , $\tan \delta$). These are found to slightly increase and σ_{ac} decreases with temperature for any frequency. The activation energy for conduction decreased with the increase in nickel oxide content (Table 7), which proved the increase in the value of interfacial polarization.

The progressive rise in modifying ion concentration generates wrong bonds in the glass network. These defects cause rather easy movement of charges, thereby enhancing interfacial polarization and hence increasing the values of dielectric parameters.

Figure 10 depicts the variation of ac conductivity with the content of nickel oxide; the curves produced a maximum for pure glass and minimum for $x = 1.0\text{ mol\%}$. The trend of the curves justified the electronic conductivity and a fixed value of ionic conductivity due to Pb^{2+} ions and Ni^{2+} ions. As the nickel oxide content increases, more Ni^{2+} ions are released into the glass network. The hopping polarons, which participate in conduction, are grabbed by Ni^{2+} ions in pairs. This combination of cation–polaron pairs diffuse as single neutral units. Movement of these neutral units cannot result in electrical conductivity so the ac conductivity decreases as the content of NiO is increased from 0.2 to 1.0 mol\% . The ionic conductivity of Pb^{2+} ions is constant in a high-temperature region. As a result of Austin and Mott's quantum mechanical tunneling model, the low-temperature part of conductivity can be explained [37]. From the results of dielectric properties, it is suggested that the significance of insulating nature is decreased with increasing content of nickel oxide.

4. Experimental Procedure

The following chemical formulas were used to synthesize the glasses for this study:

N_0 : $40\text{PbO-}60\text{GeO}_2$

N_2 : $40\text{PbO-}59.8\text{GeO}_2$: 0.2NiO

N₄: 40PbO-59.6GeO₂: 0.4NiO

N₆: 40PbO-59.4GeO₂: 0.6NiO

N₈: 40PbO-59.2GeO₂: 0.8NiO

N₁₀: 40PbO-59.0GeO₂: 1.0NiO

High-purity chemicals of PbO, GeO₂, and NiO (all are in mol%) are taken in powder form in a suitable proportion and well grounded. In a controlled furnace, properly stirred mixtures were melted at 1000–1100 degrees Celsius until bubble-free liquid was obtained for about 1 h. As a result, the bubble-free melt was poured into rectangular brass molds and instantly annealed at 350 °C for four hours in another furnace for avoiding air cracks in the samples. At last, glass samples are obtained. The Philips expert system was used to obtain the XRD patterns of glass specimens. The programmable VIBRA HT kit was utilized to conduct density measurements, employing Archimedes' law and O-xylene as the buoyant liquid. The optically polished samples have dimensions of 1 cm × 1 cm × 0.1 cm. A high-precision NIR spectrophotometer was used to obtain optical spectra. FTIR spectra were obtained using a standard spectrophotometer by a powdered sample of KBr pellets. The Raman spectra, photoluminescence spectra, and DSC traces are produced on standard instruments. The glasses were silver-coated for measuring electrical parameters. The coating was then exposed to a blower until it was dried. The electrical parameters were taken on a prominent LCR meter. The precision in determining the ϵ' is $\frac{1}{10^3}$ and that of loss is $\frac{1}{10^4}$.

5. Conclusions

40PbO–60GeO₂: NiO glasses were prepared with different concentrations from 0.2 to 1.0 mol%. The XRD and DSC patterns indicated no crystalline phases. The IR and Raman spectral analysis revealed that the entropy of the glass network decreased with increasing content of nickel oxide. The investigation into the optical absorption, ESR, and photoluminescence peaks has demonstrated a growing occurrence of Ni²⁺ ions within tetrahedral sites. The values of susceptibility and magnetic moments of the glass samples have indicated Ni²⁺ ion transformation from octahedral to tetrahedral sites. The electrical parameters ϵ' and $\tan \delta$ have increased and σ_{ac} increased whereas the activation energy has decreased, which proved their decreasing insulating nature with an increasing concentration of nickel oxide. Our observations are in agreement with prior studies on similar glass systems, where the introduction of transition metal oxides like NiO has been shown to enhance ionic conductivity due to the creation of non-bridging oxygen ions, which facilitate the movement of charge carriers. Therefore, an ionic conducting glass may be useful in solid electrolytes based on the studied glass system.

Author Contributions: L.V.: Conceptualization, writing—review and editing. S.M.S.: Writing, data curation. R.V.: Calculation and data procuring. K.P.: Formal analysis, editing. P.R.B.: Data analysis, editing. S.-J.K.: Formal analysis, conceptual discussion. G.N.R.: Supervision. All authors have read and agreed to the published version of the manuscript.

Funding: This work was supported by the 2024 Yeungnam University Research Grant.

Data Availability Statement: The data will be available on reasonable request from the corresponding author due to privacy.

Conflicts of Interest: The authors declare no conflicts of interest.

References

1. Rada, S.; Culea, M.; Neumann, M.; Culea, E. Structural role of europium ions in lead–borate glasses inferred from spectroscopic and DFT studies. *Chem. Phys. Lett.* **2008**, *460*, 196. [[CrossRef](#)]
2. Pisarski, W.; Goryczka, T.; Wodecka-Dus, B.; Plonska, M.; Pisarska, J. Structure and properties of rare earth-doped lead borate glasses. *Mater. Sci. Eng. B* **2005**, *122*, 94. [[CrossRef](#)]
3. El-Egili, K.; Doweidar, H.; Moustafa, Y.M.; Abbas, I. Structure and Some Physical Properties of PbO–P₂O₅ Glasses. *Phys. B* **2003**, *339*, 237. [[CrossRef](#)]

4. Marcel, P. Advanced glasses. *Ann. Chim. Sci. Matter* **2003**, *28*, 87.
5. Alderman, O.L.; Hannon, A.C.; Holland, D.; Umesaki, N. On the germanium–oxygen coordination number in lead germanate glasses. *J. Non-Cryst. Solids* **2014**, *386*, 56. [[CrossRef](#)]
6. Nouadji, M.; Ivanova, Z.G.; Poulain, M.; Zavadil, J.; Attaf, A. Glass formation, physicochemical characterization and photoluminescence properties of new $\text{Sb}_2\text{O}_3\text{-PbO-ZnO}$ and $\text{Sb}_2\text{O}_3\text{-PbO-ZnS}$ systems. *J. Alloy Compd.* **2013**, *549*, 158. [[CrossRef](#)]
7. Kashyap, R. Photosensitive Optical Fibers: Devices and Applications. *Opt. Fiber Technol.* **1994**, *1*, 17. [[CrossRef](#)]
8. Zmojda, J.; Kochanowicz, M.; Miluski, P.; Golonko, P.; Baranowska, A.; Ragi, T.; Dorosz, J.; Kuwik, M.; Pisarski, W.; Pisarska, J.; et al. Luminescent Studies on Germanate Glasses Doped with Europium Ions for Photonic Applications. *Materials* **2020**, *13*, 2817. [[CrossRef](#)] [[PubMed](#)]
9. Kuwik, M.; Kowalska, K.; Pisarska, J.; Pisarki, W.A. Spectroscopic properties of Pr^{3+} , Tm^{3+} , and Ho^{3+} in Germanate based Glass Systems modified by TiO_2 . *Materials* **2023**, *16*, 61. [[CrossRef](#)]
10. Zelniok, D.; Cramer, C.; Eckert, H. Structure/Property Correlations in Ion-Conducting Mixed-Network Former Glasses: Solid-State NMR Studies of the System $\text{Na}_2\text{O-B}_2\text{O}_3\text{-P}_2\text{O}_5$. *Chem. Mater.* **2007**, *19*, 3162. [[CrossRef](#)]
11. Iezid, M.; Legouera, M.; Goumeidane, F.; Poulain, M.; Nazabal, V.; Lebullenger, R. Glass formation in the $\text{Sb}_2\text{O}_3\text{-CdCl}_2\text{-SrCl}_2$ ternary system. *J. Non-Cryst. Solids* **2011**, *357*, 2984. [[CrossRef](#)]
12. Loiko, P.; Dymshits, O.; Zhilin, A.; Alekseeva, I.; Yumashev, K. Influence of NiO on phase transformations and optical properties of $\text{ZnO-Al}_2\text{O}_3\text{-SiO}_2$ glass–ceramics nucleated by TiO_2 and ZrO_2 . Part II. Optical absorption and luminescence. *J. Non. Cryst. Solids* **2013**, *376*, 99. [[CrossRef](#)]
13. Greaves, G.N.; Sen, S. Inorganic glasses, glass-forming liquids and amorphizing solids. *Adv. Phys.* **2007**, *56*, 1. [[CrossRef](#)]
14. Mysen, B.O.; Richet, P. *Silicate Glasses and Melts: Properties and Structure*; Elsevier: Amsterdam, The Netherlands, 2005.
15. Keppler, H.; Bagdassarov, N. The speciation of Ni and Co in silicate melts from optical absorption spectra to 1500 C. *Chem. Geol.* **1999**, *158*, 105. [[CrossRef](#)]
16. Reddy, M.S.; Krishna, G.M.; Veeraiah, N. Spectroscopic and magnetic studies of manganese ions in $\text{ZnO-Sb}_2\text{O}_3\text{-B}_2\text{O}_3$ glass system. *J. Phys. Chem. Solids* **2006**, *67*, 789. [[CrossRef](#)]
17. Nassau, K. The material dispersion zero in infrared optical waveguide materials. *Bell Syst. Technol. J.* **1981**, *60*, 327. [[CrossRef](#)]
18. Mc Cubbin, T.K., Jr.; Atmosoekarto, S.; Withstandley, V. Infrared Spectroscopy with a Copper-Doped Germanium Detector. *Appl. Opt.* **1967**, *6*, 1131. [[CrossRef](#)]
19. SrinivasaReddy, M.; Prasad, S.V.G.V.A.; Veeraiah, N. Valence and coordination of chromium ions in $\text{ZnO-Sb}_2\text{O}_3\text{-B}_2\text{O}_3$ glass system by means of spectroscopic and dielectric relaxation studies. *Phys. Status Solidi A* **2007**, *204*, 816. [[CrossRef](#)]
20. Tagiara, N.S.; Chatzipanagis, K.I.; Bradtmuller, H.; Rodrigues, A.C.M.; Moncke, D.; Kamitos, E.I. Network former mixing effects in alkali germanotellurite glasses: A vibrational spectroscopic study. *J. Alloys Compd.* **2021**, *882*, 160782. [[CrossRef](#)]
21. Rada, S.; Erhan, R.V.; Bodnarchuk, V.; Barbu-Tudoran, L.; Culea, E. SANS, RAMAN and SEM studies of lead-germanate glasses doped with the manganese oxide. *J. Alloys Compd.* **2021**, *882*, 160721. [[CrossRef](#)]
22. Mattos, G.R.S.; Bordon, C.D.S.; Kassab, L.R.P.; Issa, S.A.; AlMisned, G.; Tekin, H.O. Towards obtaining the optimum physical, optical, and nuclear radiation attenuation behaviours of tellurite-germanate glasses through Eu_2O_3 reinforcement: Glass synthesis, experimental and theoretical characterization study. *Ceram. Int.* **2023**, *49*, 986. [[CrossRef](#)]
23. Pipes, R.S.; Shelby, J.E. Formation and properties of soda lime germanate glasses. *J. Non-Cryst. Solids* **2021**, *553*, 120506. [[CrossRef](#)]
24. Falci, R.F.; Guerineau, T.; Delarosbil, J.L.; Messaddeq, Y. Spectroscopic properties of gallium-rich germane gallate glasses doped with Tm^{3+} . *J. Lumin.* **2022**, *249*, 119014. [[CrossRef](#)]
25. Jianga, X.P.; Yang, Z.M.; Liu, S.H. Energy transfer between Yb^{3+} and Er^{3+} in barium gallogermanate glass. *J. Appl. Phys.* **2009**, *105*, 103113. [[CrossRef](#)]
26. Pisarska, J.; Sołtys, M.; Górný, A.; Kochanowicz, M.; Zmojda, J.; Dorosz, J.; Dorosz, D.; Sitarz, M.; Pisarski, W.A. Rare earthdoped barium gallo-germanate glasses and their near-infrared luminescence properties. *Spectrochim. Acta A* **2018**, *201*, 362–366. [[CrossRef](#)] [[PubMed](#)]
27. Saffarini, G.; Saiter, J.M.; Matthiesen, J. Thermal stability and percolation threshold of Ge-Se-Fe glasses. *Mater. Lett.* **2007**, *61*, 432–436. [[CrossRef](#)]
28. Gandhi, Y.; Mohan, N.K.; Veeraiah, N. Role of nickel ion coordination on spectroscopic and dielectric properties of $\text{ZnF}_2\text{-As}_2\text{O}_3\text{-TeO}_2$: NiO glass system. *J. Non-Cryst. Solids* **2011**, *357*, 1193. [[CrossRef](#)]
29. Kumar, G.R.; Rao, M.K.; Srikumar, T.; Rao, M.C.; Kumar, V.R.; Veeraiah, N.; Rao, C.S. Spectroscopic, dielectric dispersion and dc conductivity studies of Sb_2O_3 doped lithium fluoroborophosphate glasses mixed with small concentrations of NiO. *J. Alloys Compd.* **2018**, *752*, 179. [[CrossRef](#)]
30. Teja, P.V.; Rajyasree, C.; Krishna, S.M.; Tirupataiah, C.; Rao, D.K. Effect of some VA group modifiers on R_2O_3 (R = Sb, Bi)– $\text{ZnF}_2\text{-GeO}_2$ glasses doped with CuO by means of spectroscopic and dielectric investigations. *Mater. Chem. Phys.* **2012**, *133*, 239. [[CrossRef](#)]
31. Beattie, I.R.; Livingston, K.M.S.; Ozin, G.A.; Renolds, D.J. Single-crystal Raman spectra of arsenolite (As_4O_6) and senarmonite (Sb_4O_6). The gas-phase Raman spectra of P_4O_6 , P_4O_{10} , and As_4O_6 . *J. Chem. Soc. A* **1970**, 449–451. [[CrossRef](#)]
32. Galeener, F.L.; Geissberger, A.E.; Ogar, G.W.; Loehman, R.E. Vibrational dynamics in isotopically substituted vitreous GeO_2 . *Phys. Rev. B* **1983**, *28*, 4768. [[CrossRef](#)]
33. Lee, J.D. *Concise Inorganic Chemistry*, 5th ed.; Blackwell Science Ltd.: Hoboken, NJ, USA, 1996.

34. Brown, A.; Gupta, V. Coordination environments of Ni²⁺ in germinate glass matrices. *Opt. Mater.* **2018**, *36*, 1262–1266.
35. Suresh, B.; Reddy, M.S.; Reddy, A.S.S.; Gandhi, Y.; Kumar, V.R.; Veeraiah, N. Spectroscopic features of Ni²⁺ ion in PbO–Bi₂O₃–SiO₂ glass system. *Spectrochim. Acta Part A Mol. Biomol. Spectrosc.* **2015**, *141*, 263. [[CrossRef](#)] [[PubMed](#)]
36. Gao, G.; Reibstein, S.; Spiecker, E.; Peng, M.; Wondraczek, L. Broadband NIR photoluminescence from Ni²⁺-doped nanocrystalline Ba–Al titanate glass ceramics. *J. Mater. Chem.* **2012**, *22*, 2582. [[CrossRef](#)]
37. Austin, I.G.; Mott, N.F. Polarons in crystalline and non-crystalline materials. *Adv. Phys.* **1969**, *18*, 657. [[CrossRef](#)]

Disclaimer/Publisher’s Note: The statements, opinions and data contained in all publications are solely those of the individual author(s) and contributor(s) and not of MDPI and/or the editor(s). MDPI and/or the editor(s) disclaim responsibility for any injury to people or property resulting from any ideas, methods, instructions or products referred to in the content.